2012 SCEC Annual Report

How much stress is accumulating on the creeping section of the San Andreas Fault?

Kaj M. Johnson
Department of Geological Sciences
Indiana University, Bloomington, Indiana

1 Summary

The creeping section of the San Andreas fault (CSAF) in central California is a proposed barrier to propagation of large earthquakes. Yet, recent studies show that that the creeping section is not entirely uncoupled but is accumulating slip deficit at a rate equivalent to a Mw=7.2-7.4 earthquake every 150 years. A critical piece to understanding earthquake potential on the CSAF is determining whether slip deficit is occurring with stress accumulation on stick-slip regions or without stress accumulation on stable-sliding regions shadowed by surrounding locked areas. We use a physical model to estimate the spatial distribution of locked, stress-accumulating areas of the fault constrained by surface creep rate measurements and GPS-derived velocities. We find that the area of the fault accumulating stress, if ruptured every 150 years, would release slip equivalent to at most a Mw = 6.75 earthquake, significantly less than the Mw=7.2-7.4 150-year-equivalent total slip deficit rate.

2 Introduction

The San Andreas Fault (SAF) accommodates much of the 39 mm/yr of motion between the Sierra Nevada-Great Valley block and the Pacific plate in central California (*Argus and Gordon* [1991]; *Titus et al.* [2006]). A 150-km long section of the SAF in central California creeps at the surface and has not produced a large earthquake historically. This central creeping section is between sections of the fault that are known to have ruptured repeatedly in large earthquakes. North of the creeping section the SAF last ruptured in the 1906 $M \sim$ 7.8 San Francisco earthquake, and south of Parkfield (Figure 1) the SAF last ruptured in the 1857 $M \sim$ 8 Fort Tejon earthquake.

It has been traditionally assumed that the creeping section of the San Andreas Fault has low potential for large earthquakes. This assumption is based on the observation that creep rates approach the long-term (geologic) slip rate of 31-37 mm/yr inferred at Wallace Creek (*Sieh and Jahns* [1984]), as well as the lack of large earthquakes in the historical record (*Toppozada et al.* [2002]). For example, the Unified California Earthquake Rupture Forecast 2 (UCERF2) assumed a maximum earthquake magnitude of 6.0 for the creeping section of the SAF (*Field et al.* [2009]). This is in contrast with the Carrizo section farther south that has ruptured multiple times in large events over the past 600 years (*Akciz et al.* [2009]; *Akçiz et al.* [2010]; *Scharer et al.* [2010]). However, this assumption of low earthquake potential should be questioned based on recent advances in numerical simulations of earthquakes suggesting that creeping regions of faults may rupture dynamically under appropriate conditions (e.g., *Noda and Lapusta* [2013]). Furthermore, it has been shown using geodetic data that the creeping section of the SAF does not slide everywhere uncoupled at the long-term SAF slip rate but rather is accumulating a slip deficit at a rate equivalent to a Mw 7.2-7.4 earthquake every 150 years (*Ryder and Bürgmann* [2008]; Maurer and Johnson [2013, submitted]). However, moment accumulation can occur on stable-sliding fault regions without stress accumulation if shadowed by surrounding locked areas. Thus it remains unclear whether or not the creeping section is accumulating stress to be released in future large earthquakes.

In this study we estimate the area of the fault that is accumulating stress by inverting GPS-derived velocities in central California and surface creep rate measurements on the SAF for the distribution of

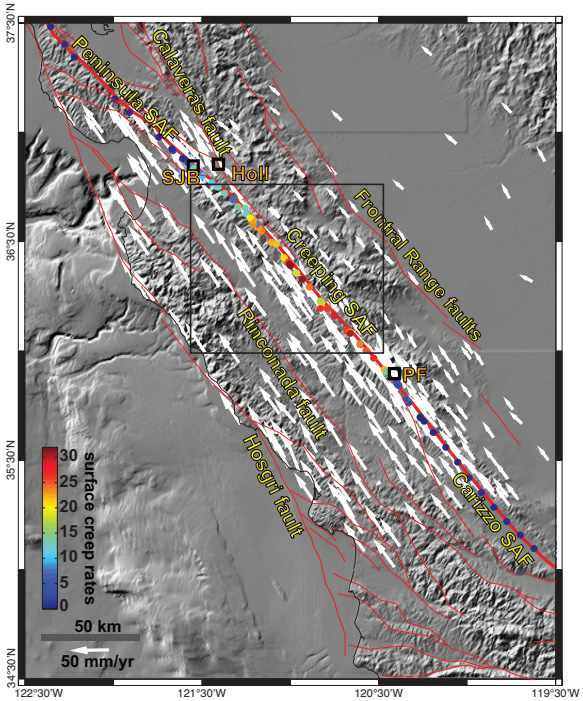

Figure 1: Digital elevation model of central California showing the active fault strands (red), GPS-derived velocity field (white vectors), and surface creep rate measurements (colored circles). Block model faults are labeled in yellow. SJB = San Juan Bautista, Holl = Hollister, PF = Parkfield.

coupling using a forward model in which the fault surface is either locked and accumulating stress or sliding at zero stressing rate.

3 Data and Methods

GPS-derived velocities from 334 stations shown in Figure 1 are taken from the Working Group for California Earthquake Probabilities UCERF3 project (UCERF3; USGS Open File Report to be released in September 2013, http://pubs.usgs.gov/of/2013/1165/). The velocities are shown in a stable North America reference frame. Direct surface creep observations show that the surface creep rate is not uniform along the CSAF (*Titus et al.* [2006]). Figure 1 shows a compilation of observed surface creep rates along the SAF demonstrating a SE to NW transition from locked (zero creep) at the surface on the Carrizo Plain section south of Parkfield to maximum surface creep rates of 25-35 mm/yr between 10 and 70 km north of Parkfield and a return to nearly zero surface creep on the Peninsula section of the SAF near San Juan Bautista. The surface creeprates are a compilation of measurements from InSAR, creepmeters, short-baseline GPS theodolite surveys, and offset cultural features (*Brown Jr and Wallace* [1968]; *Burford and Harsh* [1980]; *Louie et al.* [1985]; *Burford* [1988]; *Galehouse and Lienkaemper* [2003]; *Titus et al.* [2005]; *Tong et al.* [2013]).

We adopt the method of *Johnson and Fukuda* [2010] and solve for the distribution of locked and creeping patches and long-term fault slip rates within a plate-block model framework. Five blocks in a 30-km-thick elastic plate (crust) overlying a high-viscosity mantle are bounded by faults as illustrated in Figure 2. The Hosgri, Rinconada, San Andreas and Frontal Range faults form the block boundaries. The central SAF, Peninsula SAF, and Calaveras fault sections are discretized into slip patches nominally of length (along strike) 1.9 km and 1.7 km in width. The surface velocity field in the plate plate-block model is the sum of a long-term, steady velocity field and an interseismic perturbation to the velocity field due to coupling along faults. This is a backslip model in which interseismic fault coupling is computed with backwards slip on fault patches assuming locked patches have zero slip during the interseismic period

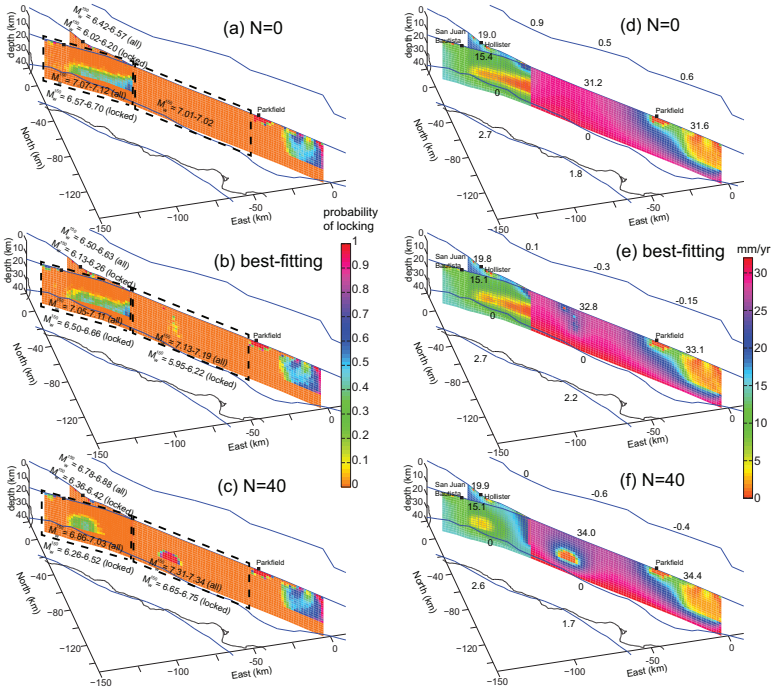

Figure 2: Model geoemtry and estimates of locking and interseismic creep rates. Blue lines show model faults (block boundaries) which correlate with names faults in Figure 1. (a-c) Color indicates the probability that a patch is locked for three different inversions (N is number of locked patches in constrained inversions). (d-f) Distribution of interseismic creep rate for three inversions. Mean of MCMC distributions. Numbers indicate long-term right-lateral fault slip rate in mm/yr (positive is right lateral).

and creeping patches slide at zero stressing rate (constant stress). In the forward model, fault patches are assigned a binary parameter (locked or creeping). Locked patches are forced to slide backwards at the long-term fault slip rate and we solve for the backslip rate on creeping patches that cancels imposed stresses due to locked patches. For this study we neglect time-variable mantle flow and compute steady interseismic stressing rates on the fault in a homogeneous elastic half space with Poisson ratio of 0.25. This is equivalent to assuming the mantle relaxation time is longer than the repeat time of earthquakes on the SAF (e.g., *Savage and Prescott* [1978]) which is not unreasonable for typical repeat times of M6 earthquakes and typically-inferred average upper mantle relaxation times in the western U.S. of order 25-250 years (e.g., *Thatcher and Pollitz* [2008]). We simultaneously solve for the long-term fault slip rates and the binary locking parameters using the Monte Carlo Metropolis algorithm. Although the faults are discretized to 30 km depth, locking is not allowed below 20 km. We refer to this method as LOCS (Locked or Constant Stress). We also conduct a sequence of constrained LOCS inversions in which the number of locked patches (but not the locations) on the creeping section is effectively fixed by introducing a prior distribution on the number of locked patches, N, assuming a Gaussian distribution with mean N and small standard deviation. The LOCS method differs from the purely kinematic backslip inversions by *Ryder and Bürgmann* [2008] and Maurer and Johnson [2013, submitted] in that LOCS distinguishes between areas of the fault that are stuck and accumulating stress and areas that creep to prevent the build up of stress. LOCS is modeled after the method established by *Bürgmann et al.* [2005] for modeling interserseismic creep at constant stress surrounding locked patches. *Hetland and Simons* [2010] considered interseismic creep and stress shadowing surrounding imposed locked areas on a fault with rate-state friction.

4 Results

The normalized chi-squared value is plotted as a function of the number of locked patches in Figure 3a. Here normalized chi-squared value is defined as the sum of squared residuals weighted by formal uncertainties and divided by the number of observations. The horizontal dashed red line shows the boundary between inversion results that fit the data equally well in a qualitative sense and models that do not fit the data well.

The probability of a patch being locked is plotted in Figure 2a-c and the mean interseismic slip rate distribution is plotted in Figure 2d-f for the best-fitting inversion and the two extreme models that fit the data satisfactorily (N=0, N=40). Here we refer to the inversion with no prior as the "best-fitting" model. All models show reduced present-day creep rates on the CSAF compared to the estimated long-term rate of 31-34 mm/yr. For the N=0 model, the reduced present-day creep rate occurs without stress accumulation and is entirely due to stress shadowing of the CSAF from the locked Carrizo/Parkfield section to the south and locking on the Peninsula SAF section to the north. The best-fitting model shows a splattering of stuck areas accumulating stress between about 5 and 15 km depth approximately 60 km NW of Parkfield that further reduces the present-day creep rate on the CSAF. The N=40 model places a 10 km $\times$ 20 km locked patch at about the same location along the CSAF but at a greater depth of $\sim 10 - 20$ km.

The predicted surface creep rate patterns are of course different for each of these models (Figure 3b) but given the scatter in the surface creep rate measurements, the N=0,40 and best-fitting models are all consistent with the observations. However, the N=80,160 models underpredict many of the measured surface creep rates along the CSAF. Inspection of the residual vectors shows that the N=0,40 and best-fitting models fit the data nearly equally well, qualitatively (or equally poorly in some cases). The N=0,40 and best-fitting residuals are most different at sites within about 5-10 km of the fault suggesting a denser set of near-fault geodetic observations might allow discrimination between these models in the future. The N=80,160 models with larger locked areas introduce significantly large residuals with a systemic right-lateral sense of residual motion of the CSAF indicating too much coupling on the fault. The large chi-squared values (Figure 2a) reflect the relatively poor fit to many of the surface creep rate measurements with rather small formal errors of order 1 mm/yr (Figure 3b).

The 99% confidence intervals of estimated moment accumulation rate are converted to 150-year-equivalent moment magnitude rates for each fault segment as shown in Figure 2 (assuming elastic shear modulus of 30 GPa). We distinguish between moment accumulation rate on locked patches and total moment accumulation rate on all patches. The range of total 150-year-equivalent moment magnitude rates for the CSAF of Mw=7.01-7.34 is similar to previous studies (*Ryder and Bürgmann* [2008]; Maurer and Johnson, submitted). However the moment magnitude rate of up to Mw=6.75 per 150 years on locked patches is substantially lower, equivalent to at most 40% of the total moment accumulation rate. This is also true for the Peninsula section of the SAF with total moment magnitude rates of Mw=6.86-7.12 per 150 years for all patches and Mw=6.26-6.7 per 150 years on locked patches.

5 Discussion and Conclusions

Ryder and Bürgmann [2008] and Maurer and Johnson [2013, submitted] both suggested that although there may be a significant moment accumulation rate on the creeping section of the SAF, it was unclear whether or not this accumulating moment would be released seismically or aseismically in the future. We have taken these analyses a step further using a physically-constrained model for interseismic creep and we find that the actual area of the CSAF that is locked and accumulating stress is small and the moment accumulation rate on the locked areas is at most 40% of the total moment accumulation rate over the entire creeping section. Although there is no explicit fault rheology in this stress-driven creep model, if one were to adopt a viscous or rate-strengthening friction rheology for the creep process the result would be the same for the case of steady interseismic sliding because stress would not accumulate on the fault with such rheologies. In the framework of rate-state friction, our locked patches would correspond with areas of velocity-weakening friction (potentially unstable) and creeping patches would correspond with velocity-strengthening regions (conditionally stable).

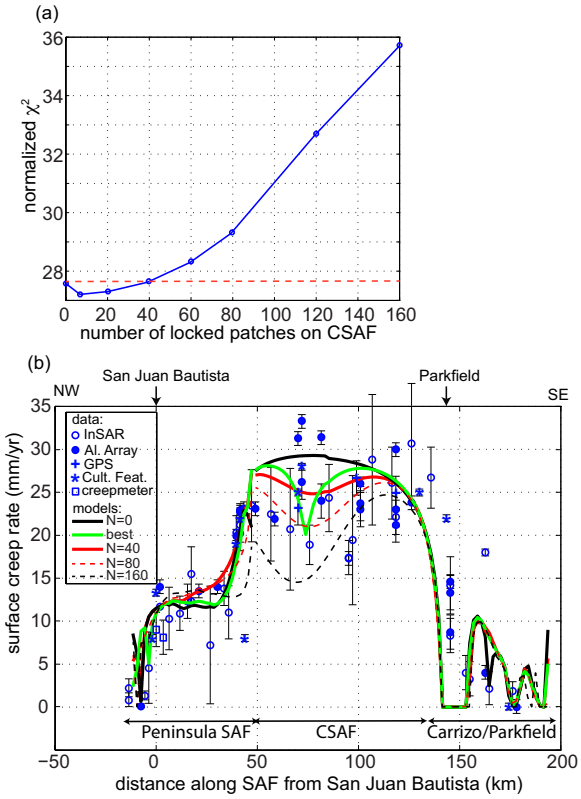

Figure 3: (a) Normalized chi-sqaured value for a sequence of inversions with the number of locked patches on the creeping section constrained. Dashed red line shows boundary between inversions that fit the data equally well in a qualitative sense and models that do not fit the data. (b) Observations of surface creep rate with distance along the SAF from San Juan Bautista. N is the number of constrained locked patches and "best" indicates the best fitting model.

With this simplified physical model for interseismic creep we cannot make any predictions about the area of the fault that would actually rupture in an earthquake. However, *Kaneko et al.* [2010] ran relevant numerical simulations using models with rate-state friction in which they examined the likelihood that rupture on a velocity-weakening patch would rupture dynamically through a velocity-strengthening barrier into another velocity weakening region. They showed that the intervening velocity-strengthening region becomes effectively a permanent barrier to through-going rupture for certain friction and normal stress conditions if the velocity weakening regions have enough separation. If we take typical values of friction parameter $\sigma(a-b) = 0.1-0.3$ MPa (where σ is normal stress and $a-b$ is the rate-strengthening parameter) as has been inferred from various afterslip studies at Parkfield (e.g., *Barbot et al.* [2009]), the *Kaneko et al.* [2010] result predicts that this separation distance is 40 km. We note that the separation of locked patches on the CSAF and locked patches on the Peninsula and Parkfield/Carrizo segments in our model results (Figure 2) is 40-60 km indicating low likelihood that the CSAF locked patches would rupture together with locked sections north or south of the creeping section. Yet, *Kaneko et al.* [2010] did not include any dynamic weakening mechanisms in their numerical simulations. It has been shown that under certain conditions velocity-strengthening regions can rupture dynamically. For example, *Noda and Lapusta* [2013] showed that velocity-strengthening regions of the fault can slide quasi-steadily for long periods of time and also rupture occasionally under coseismic weakening due to rapid shear heating of pore fluids. Numerical simulations with dynamic weakening would be required to further assess the likelihood of large earthquake ruptures on the creeping SAF.

6 Publications resulting from this funding

Johnson, K. M. (2013). Is stress accumulating on the creeping section of the San Andreas fault?. Geophysical Research Letters, 40(23), 6101-6105.

Maurer, J., and K.M. Johnson (in revision). Fault coupling and potential for earthquakes on the creeping section of the Central San Andreas Fault. Journal of Geophysical Research, manuscript 2013JB010741R.

References

Akciz, S. O., L. Grant Ludwig, and J. R. Arrowsmith (2009), Revised dates of large earthquakes along the carrizo section of the san andreas fault, california, since ad 1310±30, *Journal of Geophysical Research: Solid Earth (1978–2012)*, *114*(B1).

Akçiz, S. O., L. G. Ludwig, J. R. Arrowsmith, and O. Zielke (2010), Century-long average time intervals between earthquake ruptures of the san andreas fault in the carrizo plain, california, *Geology*, *38*(9), 787–790.

Argus, D. F., and R. G. Gordon (1991), Current sierra nevada-north america motion from very long baseline interferometry: Implications for the kinematics of the western united states, *Geology*, *19*, 1085–1088.

Barbot, S., Y. Fialko, and Y. Bock (2009), Postseismic deformation due to the mw 6.0 2004 parkfield earthquake: Stress-driven creep on a fault with spatially variable rate-and-state friction parameters, *Journal of Geophysical Research*, *114*(B7), B07,405.

Brown Jr, R. D., and R. E. Wallace (1968), Current and historic fault movement along the san andreas fault between paicines and camp dix, california, in *Proceedings of Conference on Geologic Problems of San Andreas Fault System*, pp. 22–41.

Burford, R., and P. Harsh (1980), Slip on the san andreas fault in central california from alinement array surveys, *Bulletin of the Seismological Society of America*, *70*(4), 1233–1261.

Burford, R. O. (1988), Retardations in fault creep rates before local moderate earthquakes along the san andreas fault system, central california, *pure and applied geophysics*, *126*(2-4), 499–529.

Bürgmann, R., M. G. Kogan, G. M. Steblov, G. Hilley, V. E. Levin, and E. Apel (2005), Interseismic coupling and asperity distribution along the kamchatka subduction zone, *Journal of Geophysical Research: Solid Earth (1978–2012)*, *110*(B7).

Field, E. H., et al. (2009), Uniform california earthquake rupture forecast, version 2 (ucerf 2), *Bulletin of the Seismological Society of America*, *99*(4), 2053–2107.

Galehouse, J. S., and J. J. Lienkaemper (2003), Inferences drawn from two decades of alinement array measurements of creep on faults in the san francisco bay region., *Bulletin Seismological Society of America*, *93*, 2415 – 2433.

Hetland, E., and M. Simons (2010), Post-seismic and interseismic fault creep ii: transient creep and interseismic stress shadows on megathrusts, *Geophysical Journal International*, *181*(1), 99–112.

Johnson, K., and J. Fukuda (2010), New methods for estimating the spatial distribution of locked asperities and stress-driven interseismic creep on faults with application to the san francisco bay area, california, *Journal of Geophysical Research*, p. doi:10.1029/2010JB007703.

Kaneko, Y., J.-P. Avouac, and N. Lapusta (2010), Towards inferring earthquake patterns from geodetic observations of interseismic coupling, *Nature Geoscience*, *3*(5), 363–369.

Louie, J. N., C. R. Allen, D. C. Johnson, P. C. Haase, and S. N. Cohn (1985), Fault slip in southern california, *Bulletin of the Seismological Society of America*, *75*(3), 811–833.

Noda, H., and N. Lapusta (2013), Stable creeping fault segments can become destructive as a result of dynamic weakening, *Nature*, *493*(7433), 518–521.

Ryder, I., and R. Bürgmann (2008), Spatial variations in slip deficit on the central san andreas fault from insar, *Geophysical Journal International*, *175*(3), 837–852.

Savage, J., and W. Prescott (1978), Asthenosphere readjustment and the earthquake cycle, *Journal of Geophysical Research*, *83*, 3369–3376.

Scharer, K. M., G. P. Biasi, R. J. Weldon, and T. E. Fumal (2010), Quasi-periodic recurrence of large earthquakes on the southern san andreas fault, *Geology*, *38*(6), 555–558.

Sieh, K. E., and R. H. Jahns (1984), Holocene activity of the san andreas fault at wallace creek, california, *Geol. Soc. Am. Bull.*, *95*, 883–896.

Thatcher, W., and F. F. Pollitz (2008), Temporal evolution of continental lithospheric strength in actively deforming regions, *GSA Today*, *18*(4/5), doi: 10.1130/GSAT01,804–5A.1.

Titus, S. J., C. DeMets, and B. Tikoff (2005), New slip rate estimates for the creeping segment of the san andreas fault, california, *Geology*, *33*(3), 205–208.

Titus, S. J., C. DeMets, and B. Tikoff (2006), Thirty-five-year creep rates for the creeping segment of the san andreas fault and the effects of the 2004 parkfield earthquake: Constraints from alignment arrays, continuous global positioning system, and creepmeters, *Bulletin of the Seismological Society of America*, *96*(4B), S250–S268.

Tong, X., D. Sandwell, and B. Smith-Konter (2013), High-resolution interseismic velocity data along the san andreas fault from gps and insar, *Journal of Geophysical Research: Solid Earth*, pp. 1–21.

Toppozada, T., D. Branum, M. Reichle, and C. Hallstrom (2002), San andreas fault zone, california: M 5.5 earthquake history, *Bulletin of the Seismological Society of America*, *92*(7), 2555–2601.